Nuclear versus electronic ring currents in oriented torsional molecules induced by magnetic fields. I. Nuclear currents of toluene

Dongming Jia [1], Maria Dimitrova [2], Yuan Man [3,4,*], Dage Sundholm [2,†] and Yonggang Yang [3,4,‡]

[1] *MOE Key Laboratory for Nonequilibrium Synthesis and Modulation of Condensed Matter, School of Physics, Xi'an Jiaotong University, Xi'an 710049, China*

[2] *Department of Chemistry, Faculty of Science, University of Helsinki, P.O. Box 55, A.I. Virtasen aukio 1, 00014 Helsinki, Finland*

[3] *State Key Laboratory of Quantum Optics and Quantum Optics Devices, Institute of Laser Spectroscopy, Shanxi University, Taiyuan 030006, China*

[4] *Collaborative Innovation Center of Extreme Optics, Shanxi University, Taiyuan 030006, China*

(Received 8 February 2022; accepted 8 September 2022; published 3 October 2022)

We develop the theory of nuclear ring currents induced by external magnetic fields in torsional molecules. The theory is applied to toluene, whose torsion axis is oriented along the magnetic field. We obtain magnetically induced diatropic and paratropic contributions to the nuclear ring current flowing in the classical and nonclassical directions, respectively. In the electronic and torsional and rotational ground state of toluene, the strengths of the diatropic and paratropic nuclear ring-current susceptibilities are −19.9 pA/T and 0.4 fA/T, respectively, yielding a net current strength of −19.9 pA/T. The paratropic contribution is very small because the torsional barrier of toluene is very low. The study suggests criteria for observing significant magnetically induced nuclear ring currents in torsional molecules whose axis is oriented along the magnetic field.

DOI: 10.1103/PhysRevA.106.042801

I. INTRODUCTION

This work is motivated by a recent discovery that external magnetic fields can induce torsional angular momenta in molecules consisting of two fragments (A and B) that can rotate around an intramolecular torsion axis [1]. Depending on the height of the torsion barrier, A can rotate relative to B. Moreover, the entire molecule can rotate around the axis. For example, the molecular structure of toluene in Fig. 1 consists of the methyl group ($A = CH_3$) and the phenyl group ($B = C_6H_5$) that can rotate around a torsion oriented along the external magnetic field [2]. The torsion axis is the molecular principal axis which coincides nearly perfectly with the shared C—C bond. The field induces rotation of the CH_3 and C_6H_5 groups around the torsion axis since the torsion barrier is very low. The rotations of the two groups are associated with magnetically induced torsional angular momenta [1]. The nuclei rotating with the two fragments generate a magnetically induced nuclear ring current, which is investigated here for the torsional and rotational ground state of toluene. The aim is to develop the theory, determine the strength of the nuclear ring currents, and assess whether the total nuclear current consists of diatropic and paratropic contributions as in the case of electronic ring currents.

Methods for calculating magnetically induced electronic current densities have been developed and employed in studies of molecular aromaticity and electron delocalization pathways [3–13]. In aromaticity studies, the magnetic field is usually applied perpendicular to aromatic rings such as the phenyl ring of toluene. Magnetically induced electronic current densities consist of diatropic and paratropic contributions flowing in the classical and nonclassical directions, respectively. Here the magnetic field is parallel to the ring, implying that the current-density flux is perpendicular to the ring. An aim of this study is to discover analogous partitioning of nuclear probability current densities. Since electrons and nuclei have opposite charges, the electronic and nuclear diatropic current densities flow in opposite directions. The same holds for paratropic current densities.

Another aim is to elucidate whether one can observe significant or even dominant magnetically induced nuclear ring currents in comparison to the magnetically induced electronic ring currents. Strong nuclear ring currents are expected for molecules with a low torsional barrier, since their fragments can rotate almost freely with respect to each other. We have chosen toluene in this study because it fulfills this criterion. The quantum-mechanical probabilities of observing the eclipsed or the staggered conformations of toluene are practically the same [14].

This paper is organized as follows. Section II presents the model, the theory, and the numerical methods. Section III discusses the results obtained for toluene in its torsional or rotational ground state. The results are summarized and conclusions are drawn in Sec. IV.

II. MODEL, THEORY, AND METHODS

In the derivation of the expression for calculating nuclear ring currents, we assume that the Born-Oppenheimer

*Also known as Jörn Manz.
†sundholm@chem.helsinki.fi
‡ygyang@sxu.edu.cn

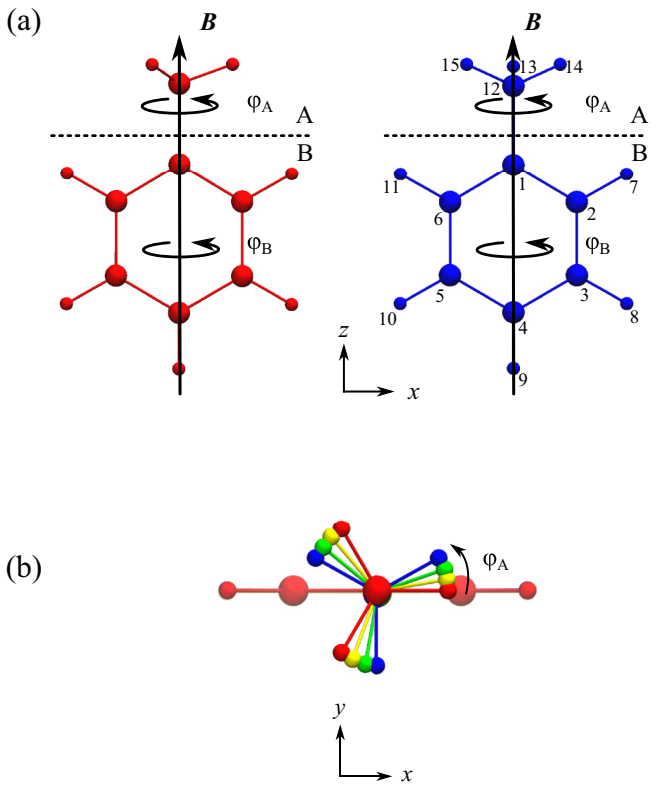

FIG. 1. Toluene with its torsion axis oriented along the external magnetic field $\boldsymbol{B}$ in the $\boldsymbol{e}_z$ direction. The nuclear center of mass is at the origin of laboratory fixed Cartesian coordinates x, y, and z. The orientation of the methyl (A) and phenyl (B) groups are defined by the rotation angles φ_A and φ_B. (a) The left and right images show the eclipsed and staggered conformers, with the (x, z) and (y, z) planes as the C_s symmetry plane, respectively. The numbering k = 1–6, 12, 7–11, and 13–15 denotes the nuclei of the C1–C6 and C7 carbon and H1–H5 and H6–H8 hydrogen atoms, respectively. The coordinates of the molecular structures are given in Tables A–D of the Supplemental Material [2]. (b) Toluene with torsion angles of $\varphi_B = 0^\circ$ and $\varphi_A = 0^\circ$ (eclipsed), $\varphi_A \approx 10^\circ$, $\varphi_A \approx 20^\circ$, and $\varphi_A \approx 30^\circ$ (staggered), seen along the torsion axis.

approximation (BOA) holds. The wave function for the torsional and rotational motions is obtained by solving the time-independent Schrödinger equation with periodic boundary conditions for the torsional and rotational motion of the fragments [15]. The BOA potential energy surface of the torsional motion is considered, whereas all other nuclear degrees of freedom are neglected.

A. A torsional molecule oriented along the magnetic field

We assume that the nuclear center of mass of molecule AB is at the origin of a right-handed Cartesian coordinate system (x, y, z) in the laboratory frame. The homogeneous external magnetic field $\boldsymbol{B} = B_z\boldsymbol{e}_z$ is oriented along the unit vector $\boldsymbol{e}_z$. The torsion axis is also along $\boldsymbol{e}_z$ with the fragments A and B with small and large moments of inertia I_A and I_B pointing in the positive and negative z directions, respectively. Angles φ_A and φ_B representing the rotation around the axis are given in degrees in the range of $0^\circ \leqslant \varphi_A, \varphi_B \leqslant 360^\circ$. The eclipsed and staggered structures shown in Fig. 1 correspond to $\varphi_A = \varphi_B = 0.0^\circ$ and to $\varphi_A \approx 30^\circ$ and $\varphi_B = 0.0^\circ$, respectively. The structures belong to the C_s point group with the (x, z) and (y, z) planes as reflection planes, respectively. The principal axes, i.e., the axes diagonalizing the moment of inertia tensor, are oriented along the laboratory x, y, and z axes such that the principal z axis coincides with the torsion axis.

The Cartesian and cylindrical coordinates (X_{Ak}, Y_{Ak}, Z_{Ak}) and $(R_{Ak}, \varphi_{Ak}, Z_{Ak})$, and (X_{Bk}, Y_{Bk}, Z_{Bk}) and $(R_{Bk}, \varphi_{Bk}, Z_{Bk})$, of the positions of the atomic nuclei in the fragments A (A_k) and B (B_k) with nuclear masses M_{Ak} and M_{Bk} and charges Q_{Ak} and Q_{Bk} are given in Tables A–D of the Supplemental Material [2]. Here R_{Ak} (R_{Bk}) is the radial distance of nucleus A_k (B_k) from the torsion axis and Z_{Ak} (Z_{Bk}) is its z coordinate. The atomic labels are defined in Fig. 1 as well as in [2]. The employed nuclear masses are $1.0079u$ for ^{1}H and $12.000u$ for ^{12}C. The corresponding charges of the bare-nucleus model employed are $1e$ and $6e$ for H and C, respectively.

The Cartesian coordinates are replaced by cylindrical coordinates whose φ_B and φ_A angles are defined as [16,17]

$$\varphi_A = \frac{\sum_k M_{Ak}R_{Ak}^2\varphi_{Ak}}{\sum_k M_{Ak}R_{Ak}^2} - 120^\circ, \quad \varphi_B = \frac{\sum_k M_{Bk}R_{Bk}^2\varphi_{Bk}}{\sum_k M_{Bk}R_{Bk}^2} - 90^\circ. \tag{1}$$

In the optimized structures, the carbon and hydrogen atoms of the phenyl group are located almost in the (x, z) plane. The nuclei of the *para*, *ipso*, and methyl carbon atoms, as well as the nucleus of the hydrogen atom in the *para* position, are practically on the torsion axis with small deviations of less than 0.015 Å caused by steric interactions. The torsional angle $\varphi = \varphi_A - \varphi_B$ corresponds to the dihedral angle $\angle\mathrm{HCCC} \equiv \mathrm{H_{methyl}} - \mathrm{C_{methyl}} - \mathrm{C_{ipso}} - \mathrm{C_{ortho}}$. The φ and $\angle$HCCC values are almost identical. In the optimization of the molecular structures, we assume $\angle\mathrm{HCCC} = 0^\circ, 10^\circ, 20^\circ, 30^\circ$ and use Eq. (1) to calculate the mass-weighted φ_A, φ_B, and φ of -0.01°, 9.91°, 19.86°, and 30.03°. The deviations are mainly due to tiny distortions of the optimized molecular structure from the ideal one.

The z components of the canonical angular momenta conjugate to φ_A and φ_B are [1,16]

$$l_{zA} = -i\hbar\frac{\partial}{\partial\varphi_A}, \quad l_{zB} = -i\hbar\frac{\partial}{\partial\varphi_B}, \tag{2}$$

where $\hbar = \frac{h}{2\pi}$ is the Dirac constant. The model neglects couplings to the other nuclear degrees of freedom, implying that fragments A and B are rigid with constant moments of inertia which are given by

$$I_A = \sum_k{}' I_{Ak}, \quad I_B = \sum_k{}' I_{Bk}, \tag{3}$$

with

$$I_{Ak} = M_{Ak}R_{Ak}^2, \quad I_{Bk} = M_{Bk}R_{Bk}^2. \tag{4}$$

The summations in Eq. (3) and in subsequent summations marked with a prime exclude the nuclei close to the torsion axis. We also introduce the relative contributions c_{Ak} and c_{Bk} to the moments of inertia

$$c_{Ak} = \frac{I_{Ak}}{I_A}, \quad c_{Bk} = \frac{I_{Bk}}{I_B}, \tag{5}$$

which are normalized as

$$\sum_k{}' c_{Ak} = 1, \quad \sum_k{}' c_{Bk} = 1. \tag{6}$$

The corresponding nuclear charges of the rotating parts of fragments A and B are

$$Q_A = \sum_k{}' Q_{Ak}, \quad Q_B = \sum_k{}' Q_{Bk}. \tag{7}$$

The related reduced and total moments of inertia for the torsion and the overall rotation are

$$I_{\rm red} = \frac{I_A I_B}{I_{\rm tot}}, \tag{8}$$

with $I_{\rm tot} = I_A + I_B$. The torsion and rotation angles

$$\begin{aligned} \varphi &= \varphi_A - \varphi_B, \\ \Phi &= \frac{I_A}{I_{\rm tot}}\varphi_A + \frac{I_B}{I_{\rm tot}}\varphi_B \equiv \eta_A\varphi_A + \eta_B\varphi_B \end{aligned} \tag{9}$$

correspond to the z components of the canonical torsional and the overall rotational angular momenta of the torsional molecule,

$$\begin{aligned} l_z &= -i\hbar\frac{\partial}{\partial\varphi} = \eta_B l_{zA} - \eta_A l_{zB}, \\ L_z &= -i\hbar\frac{\partial}{\partial\Phi} = l_{zA} + l_{zB}. \end{aligned} \tag{10}$$

The interaction of the nuclei of the torsional molecule with the magnetic field $\boldsymbol{B}$ in the $\boldsymbol{e}_z$ direction is

$$-\boldsymbol{\mu}_n\boldsymbol{B} = -\mu_{nz}B_z, \tag{11}$$

where $\boldsymbol{\mu}_n$ is the nuclear magnetic moment and μ_{nz} is its z component. In analogy with the total moment of inertia in Eq. (8), μ_{nz} can also be expressed as a sum of the contributions of the fragments A and B,

$$\mu_{nz} = \mu_{zA} + \mu_{zB}, \tag{12}$$

which are related to the z components of the canonical angular momenta of the fragments A and B as [1]

$$\begin{aligned} \mu_{zA} &= \frac{\mu_N}{\hbar} g_A l_{zA}, \\ \mu_{zB} &= \frac{\mu_N}{\hbar} g_B l_{zB}, \end{aligned} \tag{13}$$

where μ_N is the nuclear magneton $\mu_N = \frac{e\hbar}{2m_p}$. The g factors are given by [1]

$$\begin{aligned} g_A &= \sum_k{}' g_{Ak} c_{Ak}, \\ g_B &= \sum_k{}' g_{Bk} c_{Bk}, \end{aligned} \tag{14}$$

where

$$\begin{aligned} g_{Ak} &= \frac{Q_{Ak}/e}{M_{Ak}/m_p}, \\ g_{Bk} &= \frac{Q_{Bk}/e}{M_{Bk}/m_p}. \end{aligned} \tag{15}$$

Rotations of the fragments A and B with the angles φ_A and φ_B around the torsion axis of molecule AB exposed to a magnetic field $\boldsymbol{B} = B_z\boldsymbol{e}_z$ are described by the model Hamiltonian

$$H(\varphi_A, \varphi_B; B_Z) = H_R(\varphi_A, \varphi_B) - \mu_{nz}(\varphi_A, \varphi_B)B_z, \tag{16}$$

which was derived in Chap. IIa of the Supplemental Material of Ref. [1]. The field-free torsional or rotational Hamiltonian

$$\begin{aligned} H_R(\varphi_A, \varphi_B) &= \frac{l_{zA}^2}{2I_A} + \frac{l_{zB}^2}{2I_B} + V_R(\varphi_A, \varphi_B) \\ &\equiv T_R(\varphi_A, \varphi_B) + V_R(\varphi_A, \varphi_B) \end{aligned} \tag{17}$$

accounts for the torsional and rotational kinetic (T_R) and potential (V_R) energies of molecule AB. The interaction potential of the fragments A and B is modeled as

$$V_R(\varphi_A, \varphi_B) = 0.5V_b\{1 + \cos[N_{\rm GM}(\varphi_A - \varphi_B)]\}, \tag{18}$$

where $N_{\rm GM}$ is the number of equivalent periodic global minima (GMs) ($V_R = 0$), which are separated by equivalent transition states (TSs) ($V_R = V_b$) with a barrier height of V_b. One GM and one TS are shown as the staggered and eclipsed conformers of toluene in the right and the left image of Fig. 1(a), respectively. All GMs and TSs are obtained by rotating the φ_A angle with 0°, 120°, and 240° and the φ_B angle with 0° and 180°. The number of global minima $N_{\rm GM}$ and transition states $N_{\rm TS}$ of toluene is 6, which are at $\varphi = \varphi_A - \varphi_B = 30° + (k-1)\times 60°$ and at $\varphi_A - \varphi_B = (k-1)\times 60°$, with k = 1–6, as shown in Fig. 1. The corresponding cyclic molecular symmetry group is $C_6(M)$ [14].

The model Hamiltonian in Eqs. (16)–(18) is reminiscent of the Hamiltonian of two coupled coaxial quantum rings. However, Eqs. (16)–(18) can be used for describing coupled quantum rings only in the case when each ring contains a single electron, whereas quantum-ring studies generally focus on multielectron systems [18,19]. The coupling of the two electrons in the quantum rings is mediated by the repulsive Coulomb interaction leading to a different interaction potential. We also apply a homogeneous coaxial magnetic field, whereas in studies of quantum-ring systems the rings are usually exposed to inhomogeneous magnetic fields [18–21].

The Hamiltonian in Eq. (16) can be rewritten using the Φ and φ [Eq. (9)] coordinates and the conjugate total and reduced canonical angular momenta L_z and l_z [Eq. (10)]. The Hamiltonian can then be separated into the overall rotation and the torsion parts,

$$\begin{aligned} H(\varphi_A, \varphi_B; B_z) &\equiv \tilde{H}(\Phi, \varphi; B_Z) \\ &= H_{\rm rot}(\Phi; B_z) + H_{\rm tor}(\varphi; B_z), \\ H_{\rm rot}(\Phi; B_z) &= \frac{L_z^2}{2I_{\rm tot}} - \frac{\mu_N}{\hbar}(\eta_A g_A + \eta_B g_B)B_z L_z, \\ H_{\rm tor}(\varphi; B_z) &= \frac{l_z^2}{2I_{\rm red}} - \frac{\mu_N}{\hbar}(g_A - g_B)B_z l_z + V_{\rm tor}(\varphi), \end{aligned} \tag{19}$$

with the torsional potential $V_{\rm tor}(\varphi)$ given by Eq. (18). The Hamiltonian and the canonical angular momentum operator L_z commute $[H, L_z] = 0$. The nuclear ring current of the torsional molecule oriented along the magnetic field can be expressed in terms of the torsional and rotational eigenfunctions of the Hamiltonian in Eq. (19) and the angular

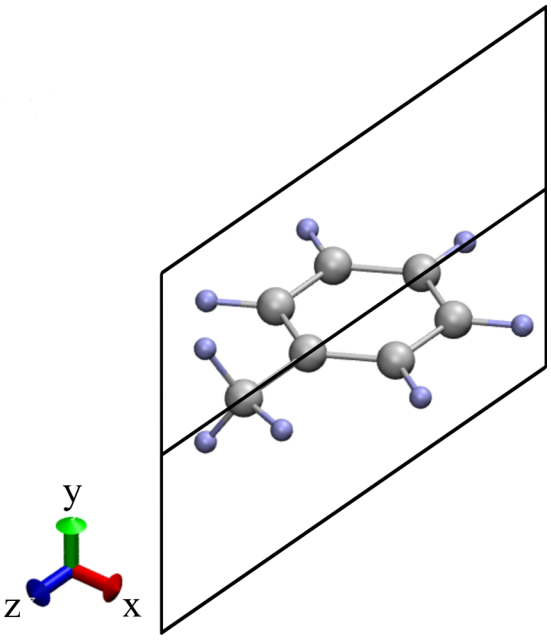

FIG. 2. Eclipsed structure of toluene with the phenyl group in the x-z plane. The upper ($y > 0$) and lower ($y < 0$) y-z half planes are shown.

momentum operator L_z in Eq. (10), with integer torsional and overall rotational magnetic quantum numbers m and M.

The eigenfunctions and eigenenergies are solutions to the corresponding time-independent Schrödinger equations

$$H(\varphi_A, \varphi_B)\, \psi_{mM}(\varphi_A, \varphi_B) = E_{mM}\, \psi_{mM}(\varphi_A, \varphi_B) \tag{20}$$

and

$$L_z\, \psi_{mM}(\varphi_A, \varphi_B) = M\hbar\, \psi_{mM}(\varphi_A, \varphi_B) \tag{21}$$

using periodic boundary conditions for φ_A and φ_B (in radians) [15],

$$\begin{aligned} \psi_{mM}(\varphi_A = 0, \varphi_B) &= \psi_{mM}(\varphi_A = 2\pi, \varphi_B), \\ \psi_{mM}(\varphi_A, \varphi_B = 0) &= \psi_{mM}(\varphi_A, \varphi_B = 2\pi). \end{aligned} \tag{22}$$

The solutions depend on the magnetic-field strength B_z, i.e., $E_{mM} \equiv E_{mM}(B_z)$ and $\psi_{mM}(\varphi_A, \varphi_B) \equiv \psi_{mM}(\varphi_A, \varphi_B; B_z)$. The model potential employed in Eq. (18) implies that the torsional and rotational energies are positive.

B. Magnetically induced nuclear ring current in torsional molecules

1. Nomenclature

Here $\mathscr{J}_n$ is the component of the nuclear current that is perpendicular to a half plane, which is fixed in the laboratory frame. One edge of the half plane coincides with the torsion axis (z axis) and the others are in principle infinitely far away from the molecule. Figure 2 shows the upper ($y > 0$) and lower ($y < 0$) y-z half planes perpendicular to the (x, z) plane corresponding to azimuthal angles equal to 90° and 270°. The $\mathscr{J}_n$ (SI unit A) is a product of the nuclear charge Q_n (SI unit C) times the probability ring current J_n (SI unit s^{-1}) of the nuclei flowing through the half plane. For torsional or rotational eigenstates, $\mathscr{J}_n$ is independent of the azimuthal angle [16], but $\mathscr{J}_n = \mathscr{J}_n^{B_z}$ depends on the magnetic-field strength B_z. The used notation is summarized in Table E of [2].

Probability ring currents J in the classical direction are clockwise. Since nuclear charges are clockwise, $\mathscr{J}_n$ and J_n have the same sign, whereas classical electronic and nuclear probability ring currents have opposite signs, due to the negative charge of electrons. The total magnetically induced nuclear ring current $\mathscr{J}_{n,\mathrm{tot}}$ in molecule AB consists of contributions from the fragments A and B,

$$\mathscr{J}_{n,\mathrm{tot}} = \mathscr{J}_{nA} + \mathscr{J}_{nB}, \tag{23}$$

which are proportional to the probability ring currents J_{nA} and J_{nB},

$$\mathscr{J}_{nA} = Q_A J_{nA}, \quad \mathscr{J}_{nB} = Q_B J_{nB}, \tag{24}$$

where Q_A and Q_B are the nuclear charges rotating with the fragments. The ring currents depend on the magnetic-field strength B_z, which we will omit in the notation. We consider one-dimensional (1D) nuclear probability ring currents, which are equal to 1D probability ring-current densities [16].

2. Derivation

Magnetically induced nuclear ring currents of torsional molecules are obtained by determining the 1D probability ring-current densities (j_{nA} and j_{nB}), which are equal to the 1D probability ring currents (J_{nA} and J_{nB}) [16], by solving the time-dependent Schrödinger equation (TDSE) with cyclic boundary conditions

$$i\hbar \frac{\partial}{\partial t} \psi(\varphi_A, \varphi_B) = H \psi(\varphi_A, \varphi_B) \tag{25}$$

and its complex conjugate. A more detailed derivation is given in Appendix A. The TDSE yields the time derivative of the nuclear probability density $\rho_n(\varphi_A, \varphi_B) = \psi^*(\varphi_A, \varphi_B)\psi(\varphi_A, \varphi_B)$, which can be inserted in the 2D rotational continuity equation for the torsional molecule AB,

$$\frac{\partial}{\partial t} \rho(\varphi_A, \varphi_B) + \frac{\partial}{\partial \varphi_A} j_A(\varphi_A, \varphi_B) + \frac{\partial}{\partial \varphi_B} j_B(\varphi_A, \varphi_B) = 0. \tag{26}$$

The derivation of Eq. (26) is analogous to the derivation of the angular continuity equation in Ref. [16]. Equations (25) and (26) yield the expression for the magnetically induced 2D rotational probability ring-current densities of torsional molecules,

$$\begin{aligned} j_A(\varphi_A, \varphi_B) = -\frac{i\hbar}{2I_A} \Bigg[& \psi^*(\varphi_A, \varphi_B) \frac{\partial}{\partial \varphi_A} \psi(\varphi_A, \varphi_B) \\ & - \psi(\varphi_A, \varphi_B) \frac{\partial}{\partial \varphi_A} \psi^*(\varphi_A, \varphi_B) \Bigg] \\ & - \frac{g_A \mu_N B_z}{\hbar} \psi^*(\varphi_A, \varphi_B) \psi(\varphi_A, \varphi_B). \end{aligned} \tag{27}$$

This expression for the angular component of the current density can also be derived by alternative approaches, e.g., as the functional derivative of the energy with respect to the magnetic vector potential [22]. A similar expression can be

derived for $j_B(\varphi_A, \varphi_B)$. The 1D rotational continuity equation for fragment A is

$$\frac{\partial}{\partial t}\rho_{nA}(\varphi_A) + \frac{\partial}{\partial \varphi_A} j_{nA}(\varphi_A) = 0, \tag{28}$$

with 1D nuclear density

$$\rho_{nA}(\varphi_A) = \int_0^{2\pi} \rho(\varphi_A, \varphi_B) d\varphi_B. \tag{29}$$

The magnetically induced 1D rotational probability ring-current density of fragment A around the torsion axis of molecule AB is given by

$$j_{nA}(\varphi_A) = \int_0^{2\pi} j_A(\varphi_A, \varphi_B) d\varphi_B \tag{30}$$

and a similar expression is obtained for $j_{nB}(\varphi_B)$. Separation of the 2D probability ring-current densities $j_A(\varphi_A, \varphi_B)$ and $j_B(\varphi_A, \varphi_B)$ into terms I and II in Eq. (27) leads to analogous separations of the 1D ones, which have an important physical meaning, as discussed below.

C. Magnetically induced nuclear ring current in the torsional ground state of toluene

The general theory of the magnetically induced probability ring current in torsional molecules can be applied to arbitrary rotational wave functions $\psi(\varphi_A, \varphi_B)$. Molecule AB in its torsional and rotational ground state $\psi_{mM}(\varphi_A, \varphi_B)$ has torsional and rotational quantum numbers $mM = 0$. Since $M = 0$, the wave function $\psi_{00}(\varphi_A, \varphi_B)$ depends only on the torsional angle $\varphi = \varphi_A - \varphi_B$. Therefore, the ground state

$$\psi(\varphi_A, \varphi_B) = \sum_{m'} c_{m'} \phi_{m'}(\varphi_A, \varphi_B) \tag{31}$$

can be expanded in orthogonal basis functions

$$\phi_{m'}(\varphi_A, \varphi_B) = \frac{1}{2\pi} e^{im'\varphi_A} e^{-im'\varphi_B}. \tag{32}$$

The summation in Eq. (31) is in principle infinite ($-\infty < m' < \infty$); however, converged results are obtained for toluene with $m_{\max} = -m_{\min} = 3606$. The Hamiltonian has, for symmetry reasons, nonvanishing off-diagonal matrix elements $H_{m'n'} = \langle \phi_{m'} | H | \phi_{n'} \rangle$ only when $m' \pm n' = N_{\mathrm{GM}}$ holds. The expressions for calculating the probability ring-current densities of fragments A and B are

$$\begin{aligned} J_{nA} &= \frac{\hbar}{2\pi I_A} {\sum_{m'>0}}' m' (|c_{m'}|^2 - |c_{-m'}|^2) - \frac{g_A \mu_N B_z}{2\pi\hbar} \\ &= J_{nA\mathrm{I}} + J_{nA\mathrm{II}}, \\ J_{nB} &= \frac{-\hbar}{2\pi I_B} {\sum_{m'>0}}' m' (|c_{m'}|^2 - |c_{-m'}|^2) - \frac{g_B \mu_N B_z}{2\pi\hbar} \\ &= J_{nB\mathrm{I}} + J_{nB\mathrm{II}}, \end{aligned} \tag{33}$$

which show that the probability ring currents of fragments A and B can be separated into two contributions [for the detailed derivation, see Eq. (A11)]. The total ring current is the sum of the A and B contributions, which can analogously be divided into parts I and II,

$$\begin{aligned} J_n &= J_{nA} + J_{nB} \\ &\equiv J_{n\mathrm{I}} + J_{n\mathrm{II}}, \\ J_{n\mathrm{I}} &= J_{nA\mathrm{I}} + J_{nB\mathrm{I}}, \\ J_{n\mathrm{II}} &= J_{nA\mathrm{II}} + J_{nB\mathrm{II}}. \end{aligned} \tag{34}$$

Contribution I depends on the torsional or rotational wave function, whereas contribution II does not. As a conjecture, this suggests that contributions I and II may be assigned as nonclassical and classical, respectively. The assignment of contribution II as classical is confirmed by the fact that it is proportional to B_z. The tentative assignment of contribution I as nonclassical implies the working hypothesis that its sign should be negative. This will be confirmed in Sec. III.

Separation of the probability ring currents into the two contributions enables an analogous separation of the total magnetically induced nuclear ring current into two parts, since the magnetically induced nuclear ring currents are obtained from the probability ring currents by multiplying them with the rotating charges Q_A and Q_B,

$$\begin{aligned} \mathscr{J}_{n,\mathrm{tot}} &= \mathscr{J}_{nA} + \mathscr{J}_{nB} = Q_A J_{nA} + Q_B J_{nB} \\ &\equiv \mathscr{J}_{n\mathrm{I}} + \mathscr{J}_{n\mathrm{II}}, \\ \mathscr{J}_{n\mathrm{I}} &= Q_A J_{nA\mathrm{I}} + Q_B J_{nB\mathrm{I}}, \\ \mathscr{J}_{n\mathrm{II}} &= Q_A J_{nA\mathrm{II}} + Q_B J_{nB\mathrm{II}}. \end{aligned} \tag{35}$$

The II terms are proportional to the strength of the external magnetic field B_z, whereas the I contributions are implicitly dependent on B_z through the expansion coefficients $c_{\pm m'}$,

$$\begin{aligned} \mathscr{J}_{n\mathrm{I}} &= \left(\frac{Q_A}{I_A} - \frac{Q_B}{I_B}\right) \frac{\hbar}{2\pi} {\sum_{m'>0}}' m' (|c_{m'}|^2 - |c_{-m'}|^2), \\ \mathscr{J}_{n\mathrm{II}} &= -(Q_A g_A + Q_B g_B) \frac{\mu_N}{h} B_z, \end{aligned} \tag{36}$$

where $m' = k\, N_{\mathrm{GM}}$ and k is a positive integer.

The nuclear ring current can be expressed as a Taylor series expansion with respect to B_z,

$$\mathscr{J}_n(B_z) = \left.\frac{\partial \mathscr{J}_n}{\partial B_z}\right|_{B_z=0} B_z + \cdots, \tag{37}$$

where the ellipsis denotes higher-order terms. The constant term vanishes when assuming that the fragments do not rotate in the absence of B_z. The nuclear ring-current susceptibility is the coefficient of the term that is linear in B_z. Higher-order contributions are neglected. The susceptibility of the magnetically induced nuclear ring current in Eq. (38) is obtained in the limit of vanishing magnetic field by differentiating Eq. (36) with respect to B_z,

$$\begin{aligned} \mathcal{J}^{B_z}_{n\mathrm{I}} &= \left(\frac{Q_A}{I_A} - \frac{Q_B}{I_B}\right) \frac{\hbar}{2\pi} {\sum_{m'>0}}' m' \left.\frac{\partial(|c_{m'}|^2 - |c_{-m'}|^2)}{\partial B_z}\right|_{B_z=0}, \\ \mathcal{J}^{B_z}_{n\mathrm{II}} &= -(Q_A g_A + Q_B g_B) \frac{\mu_N}{h} < 0. \end{aligned} \tag{38}$$

The classical contribution to the nuclear ring-current susceptibility can be calculated analytically, whereas calculations of the nonclassical part is obtained by diagonalizing the B_z-dependent Hamiltonian.

TABLE I. Comparison of calculated and experimental values for the parameters of the model Hamiltonian of toluene.

Molecular property	Results from DFT calculations[a]				Experiment
dihedral angle ∠HCCC (deg)[b]	0[c]	10	20	30[d]	
φ_A (deg)[e]	−0.01	9.91	19.86	30.03	
φ_B (deg)[e]	0.00	0.00	0.00	0.00	
torsion angle $\varphi = \varphi_A - \varphi_B$ (deg)	−0.01	9.91	19.86	30.03	
moment of inertia I_A (μÅ^2)	3.113	3.113	3.113	3.113	3.208[f]
moment of inertia I_B (μÅ^2)	87.438	87.443	87.449	87.455	84.984[f]
potential energy V (kJ/mol)	0.038[g]	0.030	0.011	0.00[h]	0.0583[i]
nuclear g factor g_A	0.992	0.992	0.992	0.992	[j]
nuclear g factor g_B	0.472	0.472	0.472	0.472	[j]

[a]Values calculated at the density-functional theory (DFT) level using the B3LYP functional and the def2-TZVP basis (cf. Appendix B).
[b]∠HCCC = H7 − C7 − C1 − C2.
[c]Eclipsed structure.
[d]Staggered structure.
[e]Calculated using Eq. (1).
[f]Taken from Ref. [14], independent of torsion angle.
[g]Barrier height $V_b = V_R(\varphi = 0)$ for the eclipsed structure.
[h]The potential minimum is set to $V_R \equiv 0$ for the staggered structure.
[i]Taken from Ref. [26].
[j]Experimental nuclear g factors are not available.

III. RESULTS AND DISCUSSION

A. Toluene structure calculations

Toluene has six equivalent global minimum structures ($N_{\mathrm{GM}} = 6$) corresponding to the staggered conformer in Fig. 1. Only five parameters are needed for describing the interactions of the toluene nuclei with an external magnetic field. The parameters are the moments of inertia I_A and I_B for rotations of the fragments A and B around the torsion axis or alternatively the total and reduced moments of inertia I_{tot} and I_{red}, the height of the torsion barrier V_b of the methyl group, and the nuclear g factors g_A and g_B of the magnetic interaction with the nuclei of the fragments A and B. The rotating nuclear charges are assumed to be $Q_A = 3e$ and $Q_B = 28e$.

For toluene, the energy range below $345hc$ cm^{-1} has been studied experimentally with high accuracy. The lowest excited methyl-rotor and vibrating-rotor states of the electronic ground state of toluene were investigated by using high-resolution 2D laser-induced fluorescence spectroscopy [14]. The experimental value of the torsion barrier V_b of $-1.57hc$ cm^{-1} is very small and negative, implying that the energy of the eclipsed toluene is energetically below the staggered structure [14]. The energy order of the eclipsed and staggered structures changes when the coupling between the torsion mode and the lowest vibrational mode was considered in the model Hamiltonian [14,23–25]. The probability distribution of the torsional wave function of toluene has its maximum at the staggered structure even though the global minimum of the experimental potential energy is for the eclipsed geometry [14]. Our model Hamiltonian does not account for this coupling. A proper torsional nuclear density can be obtained also when ignoring the coupling term if one uses a V_b of $4.874hc$ cm^{-1} that is derived from microwave spectroscopy measurements [14,26]. The effective Hamiltonian for toluene used in our calculations has a torsional potential energy curve with the global minimum for the staggered structure and a potential barrier V_b of 0.0583 kJ/mol at the eclipsed structure [26]. The employed potential barrier leads to error compensation in the calculation of the nuclear density, since it has its minimum at the staggered structure compensating for the neglected torsional-vibrational coupling. The coupling term also alters the energetic order of excited torsional or rotational and vibrating-rotor states, which cannot be reproduced by the effective potential barrier [14]. However, studies of excited torsional states are beyond the scope of this work.

We have also carried out electronic structure calculations of the torsional barrier, based on Refs. [27–33] (cf. Appendix B). The results for the potential energy are listed in Table I and the resulting Cartesian and cylindrical coordinates for the torsional ∠HCCC = 0°, 10°, 20°, 30° are given in Tables A–D of [2]. The origin of the Cartesian coordinates is at the center of mass and the principal axes point along x, y, and z. The z axis coincides with the torsion axis, which is oriented along the external magnetic field $\boldsymbol{B} = B_z\boldsymbol{e}_z$. The molecular structures are shown in Figs. 1 and 2. The moments of inertia I_A and I_B and the g factors g_A and g_B were calculated using these coordinates. The carbon nucleus of the methyl group, the *ipso* and *para* carbon atoms of the phenyl group and the *para* hydrogen atom were excluded in the calculation of moments of inertia and g factors because they are very close to the torsion axis. They were also excluded in the calculations of the magnetically induced nuclear ring currents.

The calculated and experimental moments of inertia compared in Table I agree well, whereas the ratios between them suggest that the calculated C—H bonds of the methyl group are slightly too short compared to the experimental bond length. The calculated bond length of the methyl C—H bond of 1.091 Å is 0.054 Å shorter than the one obtained in an electron-diffraction measurement [34]. The calculated length of the C—H bond of the phenyl group is 0.014 Å shorter than obtained experimentally [34], whereas the lengths of the C—C bonds agree within 0.004 Å with experimental data [34]. The small deviations are due to the level of theory em-

ployed in the electronic structure calculation and the neglect of vibrational effects. The close agreement between calculated and measured values for the moments of inertia supports the assumption of robust fragments that were used in Ref. [14]. We use the experimental I_A and I_B data [14] in the calculations of nuclear ring currents because they are slightly more accurate than the calculated ones. The same accuracy is expected for the calculated g factors as for the calculated moments of inertia.

The barrier height V_b of 0.058 kJ/mol calculated at the B3LYP/def2-QZVP level agrees well with the experimental value of 0.0583 kJ/mol [26], which we used as the effective barrier height in the modeling. Calculations at the B3LYP/def2-TZVP level yielded a lower barrier of 0.038 kJ/mol. The dependence of the strength of the nuclear ring current on the barrier height was investigated by using barriers in the range of [0,40] kJ/mol. The other molecular parameters were then kept fixed. A vanishing barrier corresponds to free rotation of the fragments around the torsion axis. The torsional motion is blocked when using the upper limit of 40 kJ/mol, whereas the whole molecule is locked in the staggered conformation that can rotate around the principal axis.

B. The torsional or rotational wave function of toluene

The ground-state torsional or rotational wave function of toluene ($mM = 0$) is $\psi(\varphi_A, \varphi_B) = \sum'_{m'} c_{m'}\phi_{m'}(\varphi_A, \varphi_B)$, where the summation is limited to $|m'| = 6k$ with $k = 0, 1, 2\ldots$ having the nonvanishing coefficients $c_{\pm 6k}$. The contributions to the nuclear ring current in Eq. (36) originate from the $k > 0$ terms. The dependence of the dominating expansion coefficients of the wave function on the barrier height and on the magnetic field strength is shown in Fig. 3, where Figs. 3(a)–3(e) show $|c_0|^2$, $|c_{+6}|^2$, $|c_{+12}|^2$, and the differences $|c_6|^2 - |c_{-6}|^2$ and $|c_{12}|^2 - |c_{-12}|^2$ as a function of V_b for four B_z strengths. Figures 3(f)–3(j) show $\Delta|c_0|^2$, $\Delta|c_{+6}|^2$, $\Delta|c_{+12}|^2$, and $|c_6|^2 - |c_{-6}|^2$ and $|c_{12}|^2 - |c_{-12}|^2$ as a function of B_z for four barrier heights. The differences $\Delta|c_{m'}|^2 = |c_{m'}|^2(B_z) - |c_{m'}|^2(B_z = 0)$ enable visualization of the B_z dependence of the $|c_{m'}|^2$ coefficients which cannot be resolved in Figs. 3(a)–3(c).

For $B_z = 0$ and $V_b = 0$, all coefficients vanish except $|c_0| = 1$. The nuclear eigenfunction is $\phi(\varphi_A, \varphi_B) = \frac{1}{2\pi}$, implying that the nuclear density is completely delocalized, i.e., all angles φ_A and φ_B are equally probable. For higher barriers, the absolute value of the c_0 coefficient decreases and the absolute values of the $|c_6|, |c_{-6}|, \ldots$ coefficients increase. At even higher barriers, the absolute values for the c_0, c_6, and c_{-6} coefficients decrease and the absolute values of c_{12} and c_{-12} and higher-order coefficients increase. In the limit $V_b \to \infty$, all coefficients are equal, corresponding to a nuclear ground-state wave function that has equivalent sharp peaks in the six potential wells. The free rotation of fragment A relative to B at $V_b = 0$ changes to a free rotation of six equivalent rigid-rotor structures when $V_b \to \infty$.

The squared coefficients with opposite quantum numbers $\pm m'$ cannot be distinguished on the graphical scale of Figs. 3(a)–3(c) because the dependence of the coefficients on the magnetic field is weak. The curves for $B_z = 0$, 3, 6, and 9 T coincide within the graphical resolution, suggesting

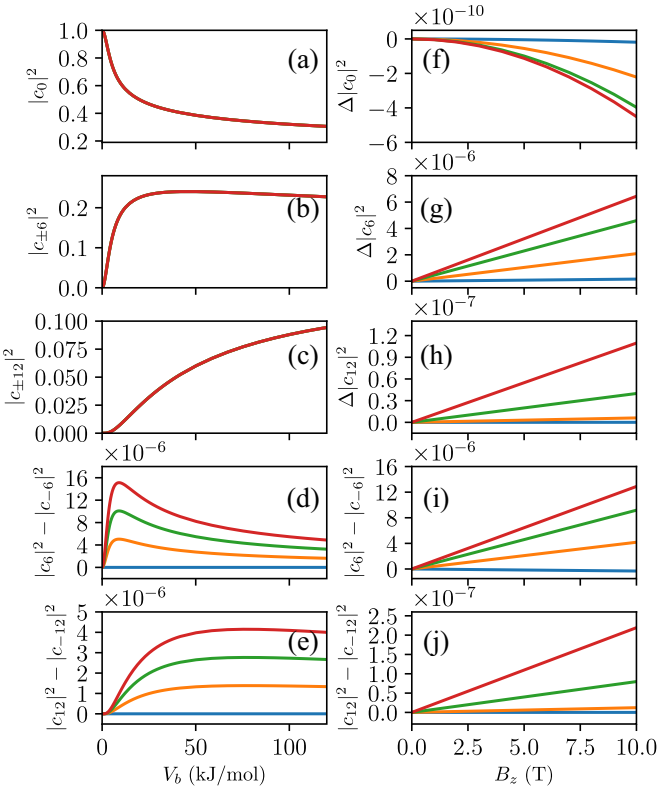

FIG. 3. Squared coefficients (a) c_0, (b) $c_{\pm 6}$, and (c) $c_{\pm 12}$ of the ground-state wave function of toluene as a function of the potential barrier V_b for magnetic-field strength B_z of 0 (blue), 3 (orange), 6 (green) and 9 T (red). The (d) $|c_6|^2 - |c_{-6}|^2$ and (e) $|c_{12}|^2 - |c_{-12}|^2$ curves are also shown. The right panels show $\Delta|c_{m'}|^2 = |c_{m'}|^2(B_z) - |c_{m'}|^2(B_z = 0)$ for (f) $m' = 0$, (g) $m' = 6$, and (h) $m' = 12$ and (i) $|c_6|^2 - |c_{-6}|^2$ and (j) $|c_{12}|^2 - |c_{-12}|^2$ as a function of B_z for barrier heights V_b of 0.4 (blue), 1.6 (orange), 2.8 (green) and 4 kJ/mol (red), respectively. The sequence of the lines for 0.4, 1.6, 2.8 and 4.0 kJ/mol is from bottom to top in panels (d), (e), (g)–(j), and vice versa in panel (f).

that the nonclassical contribution to the magnetically induced nuclear ring current is small. The magnetic dependence is seen in Figs. 3(d) and 3(e). The $|c_6|^2 - |c_{-6}|^2$ difference vanishes for $V_b = 0$ and it is positive for $V_b > 0$. The absolute value of $|c_6|^2 - |c_{-6}|^2$ increases rapidly with increasing V_b and for higher barriers it decreases but the value of $|c_6|^2 - |c_{-6}|^2$ remains positive. The same holds for the $|c_{12}|^2 - |c_{-12}|^2$ curve whose maximum is at a higher barrier than for the $|c_6|^2 - |c_{-6}|^2$ curve. The maximum of the $|c_6|^2 - |c_{-6}|^2$ curve is deeper when increasing the magnetic-field strength. The distances between the $|c_6|^2 - |c_{-6}|^2$ curves for $B_z = 0$, 3, 6, and 9 T suggest $|c_6|^2 - |c_{-6}|^2$ is nearly linearly dependent on B_z. The same holds for $|c_{12}|^2 - |c_{-12}|^2$, but it is less pronounced. The calculations show that the $|c_6|^2 - |c_{-6}|^2$ term dominates under the studied conditions.

Figures 3(f)–3(j) show that $\Delta|c_{m'}|^2 = |c_{m'}|^2(B_z) - |c_{m'}|^2(B_z = 0)$ as a function of the magnetic-field strength is nearly linear, except for $|c_0|^2$. However, the variation of $|c_0|^2$ versus B_z is negligible compared to the variation of the other coefficients. The steepest slope of the $\Delta|c_{6n}|^2$ ($n = 0, 1, 2$),

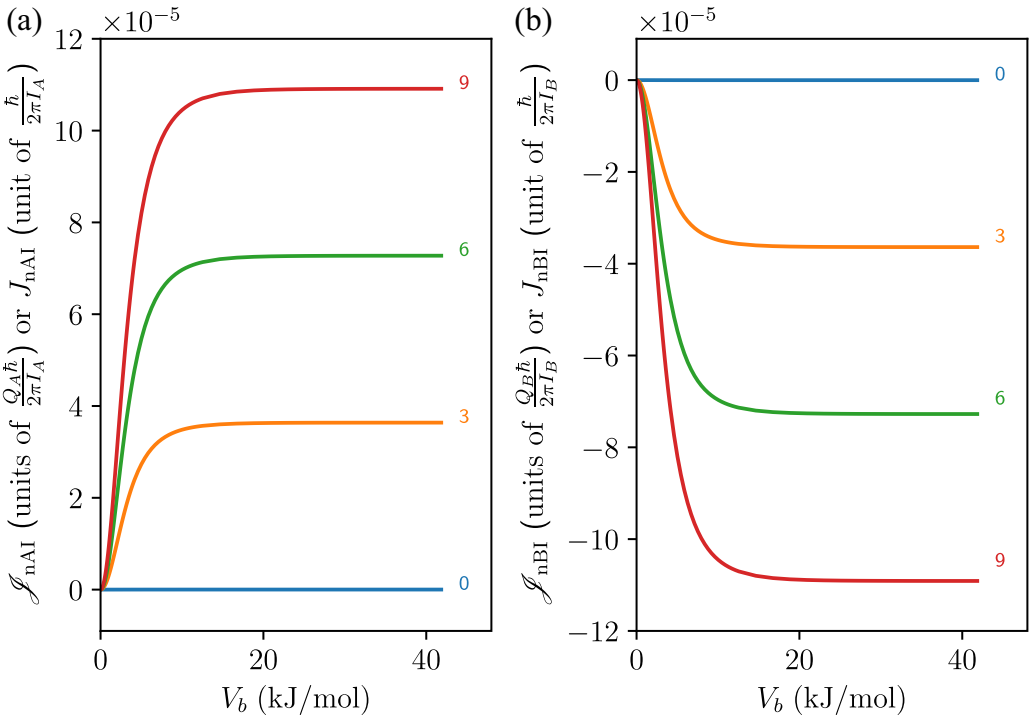

FIG. 4. Contribution from the nonclassical (I) probability ring current J or the nuclear ring current $\mathscr{J}$ of (a) the methyl (A) and (b) the phenyl (B) groups of toluene as a function of the barrier height V_b calculated for four strengths of the magnetic field: $B_z = 0$ (blue), 3 (orange), 6 (green), and 9 T (red).

$|c_6|^2 - |c_{-6}|^2$, and $|c_{12}|^2 - |c_{-12}|^2$ curves as a function of B_z is obtained for the highest barrier.

C. Magnetically induced nuclear ring currents in toluene

The magnetically induced probability ring currents and nuclear ring currents of toluene in the torsional or rotational ground state consist of contributions from the methyl (A) and phenyl (B) groups. The ring current of each fragment can be divided into classical (II) and nonclassical (I) contributions. The nonclassical contributions are obtained by using the expansion coefficient of the torsional or rotational wave function calculated as described in the preceding section. The main contribution originates from $|m'| = 6$, as shown in Figs. 3(d) and 3(i).

The calculated $J_{nA\mathrm{I}}$ and $J_{nB\mathrm{I}}$ (in units of $\frac{\hbar}{2\pi I_A}$ and $\frac{\hbar}{2\pi I_B}$, respectively) as a function of V_b and B_z are shown in Figs. 4 and 5, where we have used B_z equal to 0, 3, 6, and 9 T and V_b equal to 0.4, 1.6, 2.8, and 4.0 kJ/mol. Since the expressions for $J_{nA\mathrm{I}}$ in units of $\frac{\hbar}{2\pi I_A}$ and for $J_{nB\mathrm{I}}$ in units of $\frac{\hbar}{2\pi I_B}$ are identical, with opposite sign, as derived in Appendix A [cf. Eq. (A11)] and as seen in Eq. (33), it is sufficient to discuss the properties of the $J_{nA\mathrm{I}}$ expression

$$J_{nA\mathrm{I}} \Big/ \left(\frac{\hbar}{2\pi I_A}\right) = -J_{nB\mathrm{I}} \Big/ \left(\frac{\hbar}{2\pi I_B}\right). \tag{39}$$

Figure 5(a) shows that the dependence of $J_{nA\mathrm{I}}$ on B_z is almost linear, for all values of V_b. The linear dependence holds at least for magnetic fields below 10 T, which is accessible by standard experimental equipment. It also holds for very low rotational barriers as the present V_b value of 0.0583 kJ/mol (not shown). The slope of $J_{nA\mathrm{I}}/(\frac{\hbar}{2\pi I_A})$ as a function of B_z is steeper for higher torsion barriers as seen in Fig. 5(a) because the dominant expansion coefficients $|c_6|^2 - |c_{-6}|^2$ in Fig. 3(i) exhibit such behavior. For large barriers, $J_{nA\mathrm{I}}/(\frac{\hbar}{2\pi I_A})$ is leveling off because the torsional motion of A relative to B is blocked. The average slope of $J_{nA\mathrm{I}}/(\frac{\hbar}{2\pi I_A})$ as a function of V_b for low barriers is also steeper when the magnetic field is stronger, as seen in Fig. 4(a). This can also be traced back to the behavior of the expansion coefficients as a function of B_z in Fig. 3(d).

The nonclassical part (I) of the nuclear ring current $\mathscr{J}_{n\mathrm{I}} = \mathscr{J}_{nA\mathrm{I}} + \mathscr{J}_{nB\mathrm{I}}$ induced by the magnetic field in the methyl (A) and phenyl (B) groups is shown in Fig. 6(a) for torsion barriers of 0.4, 1.6, 2.8, and 4 kJ/mol. The classical part (II) $\mathscr{J}_{n\mathrm{II}} = \mathscr{J}_{nA\mathrm{II}} + \mathscr{J}_{nB\mathrm{II}}$ is shown in Fig. 6(b). The nuclear ring current of toluene is nearly linear with respect to the strength of the external magnetic field, as seen in Fig. 6(a). The positive slope confirms that contribution I is nonclassical. In contrast, the classical contribution II depends nearly linearly on B_z with a negative slope, as seen in Fig. 6(b). For toluene with a very small torsion barrier, the B_z dependence in Fig. 6(a) would be an almost horizontal line on the same scale.

The nonclassical (I) and classical (II) magnetically induced nuclear ring currents can therefore be assigned as paratropic and diatropic, respectively. The first contribution to $J_{n\mathrm{I}}(B_z)$ is positive and therefore nonclassical (paratropic) because the

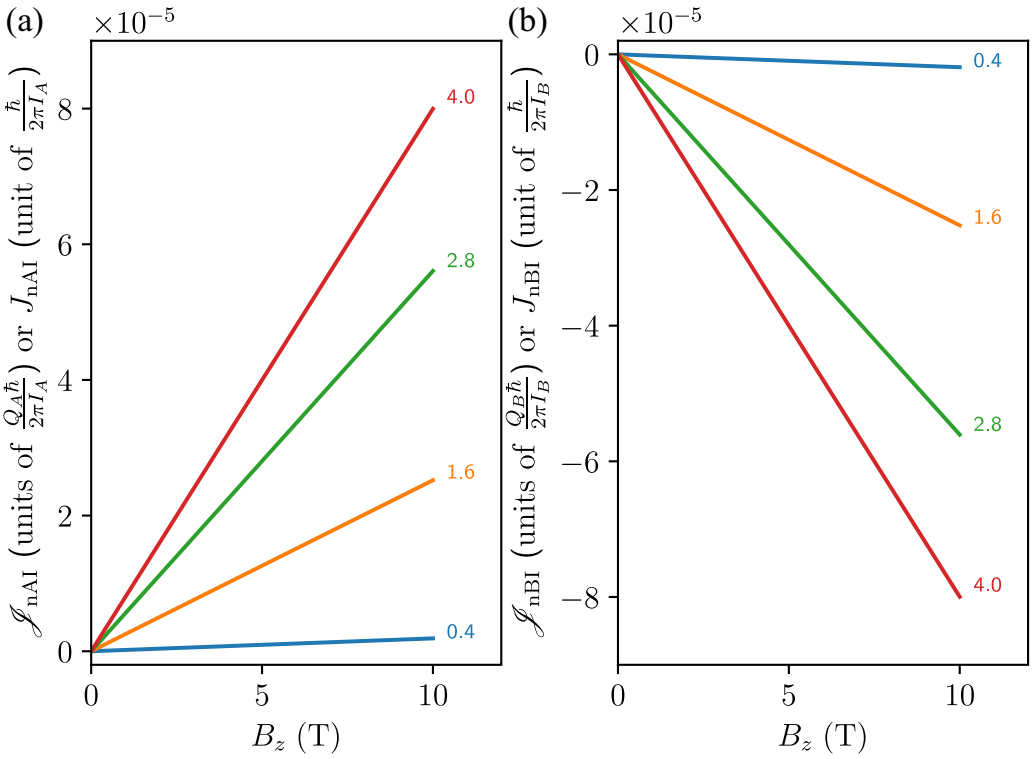

FIG. 5. Almost linear behavior of the nonclassical contribution (I) to the probability ring current J and the nuclear ring current $\mathscr{J}$ of (a) the methyl (A) and (b) the phenyl (B) groups of toluene calculated with barrier heights V_b of 0.4 (blue), 1.6 (orange), 2.8 (green), and 4 kJ/mol (red).

first factor $Q_A/I_A - Q_B/I_B$ in Eq. (36) is positive and the second factor $\sum'_{m'>0} m'(|c_{m'}|^2 - |c_{-m'}|^2)$ is also positive, as seen in Fig. 3.

The absolute value of the classical nuclear ring current is much stronger than the nonclassical one $|\mathscr{J}^{B_z}_{n\mathrm{II}}| \gg \mathscr{J}^{B_z}_{n\mathrm{I}}$. A strong magnetically induced nuclear ring current in torsional molecules can be expected when $(Q_A g_A + Q_B g_B)$ is large. The potential barrier V_b should also be small because a large V_b increases the strength of the positive nonclassical nuclear ring current, leading to a weaker total nuclear ring current. The positive contribution to the nuclear ring current vanishes when the ratios of the moments of inertia and the charges of the rotating fragments A and B are equal. For example, CH_3—CH_3 has the same I_A and I_B as well as Q_A and Q_B. If ethylene is aligned parallel to the external magnetic field, then the field will induce exclusively a diatropic nuclear ring current, without any paratropic contribution.

The nuclear ring-current susceptibility $\mathcal{J}^{B_z}_n$ is the derivatives of the nuclear ring currents with respect to the magnetic field in the limit of vanishing magnetic field. Here $\mathcal{J}^{B_z}_n$ is

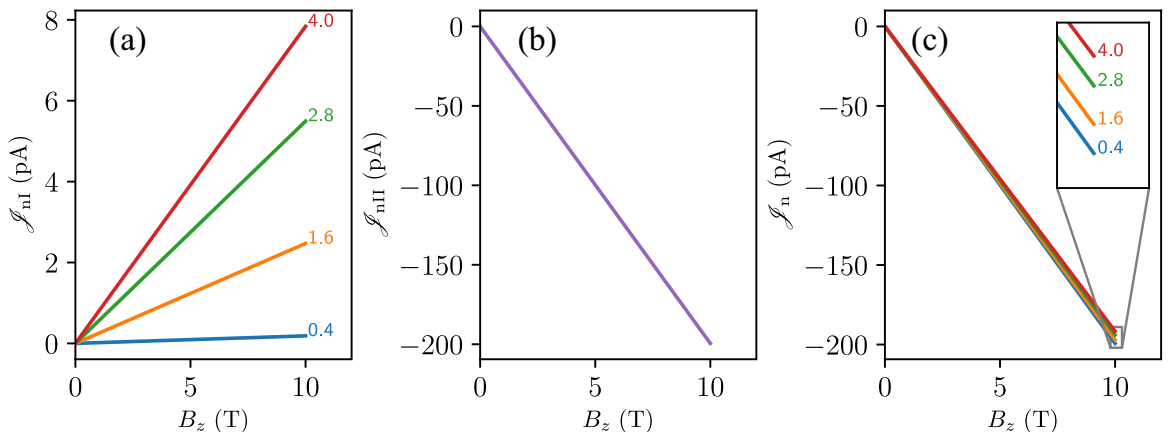

FIG. 6. (a) Nonclassical and paratropic contribution $\mathscr{J}_{n\mathrm{I}}$ to the nuclear ring current $\mathscr{J}_{n,\mathrm{tot}}$ in toluene induced by a magnetic field B_z calculated for different torsion barriers. (b) Corresponding classical and diatropic contribution $\mathscr{J}_{n\mathrm{II}}$. (c) Total nuclear ring current as a function of the magnetic-field strength B_z calculated using torsion barrier heights V_b of 0.4, 1.6, 2.8, and 4 kJ/mol.

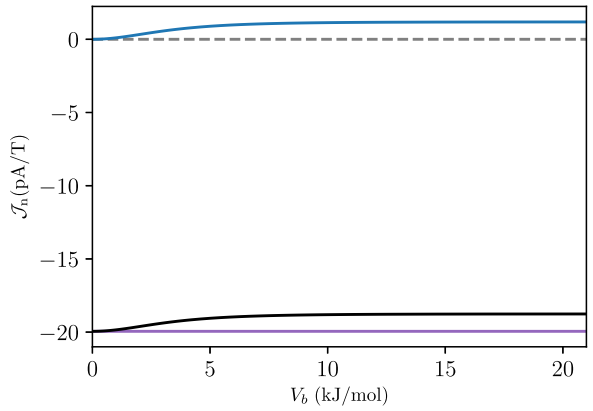

FIG. 7. Nonclassical (blue), classical (purple), and total (black) magnetically induced nuclear ring-current susceptibilities of toluene as a function of the height of the torsion barrier.

a constant because we consider only one direction of the magnetic field and the nuclear ring current is a 1D function describing the rotational nuclear charges

$$\mathcal{J}_n^{B_z} = \left.\frac{\partial \mathcal{J}}{\partial B_z}\right|_{B_z=0}. \tag{40}$$

The sum of the nonclassical nuclear ring-current susceptibilities in fragments A and B is

$$\begin{aligned}\mathcal{J}_{n\mathrm{I}}^{B_z} &= \mathcal{J}_{n\mathrm{AI}}^{B_z} + \mathcal{J}_{n\mathrm{BI}}^{B_z},\\ \mathcal{J}_{n\mathrm{II}}^{B_z} &= \mathcal{J}_{n\mathrm{AII}}^{B_z} + \mathcal{J}_{n\mathrm{BII}}^{B_z}.\end{aligned} \tag{41}$$

The total nuclear ring-current susceptibility is the sum of the nonclassical plus the classical contributions

$$\mathcal{J}_{n,\mathrm{tot}}^{B_z} = \mathcal{J}_{n\mathrm{I}}^{B_z} + \mathcal{J}_{n\mathrm{II}}^{B_z}. \tag{42}$$

The total nuclear ring-current susceptibility and the nonclassical (I) and classical (II) contributions of fragments A and B of toluene calculated using $V_b = 0.0583$ kJ/mol are

$$\begin{aligned}\mathcal{J}_{n,\mathrm{tot}}^{B_z} &= -19.946\ \mathrm{pA/T} = \mathcal{J}_{n\mathrm{I}}^{B_z} + \mathcal{J}_{n\mathrm{II}}^{B_z}\\ &= (0.402 \times 10^{-3} - 19.946)\ \mathrm{pA/T},\\ \mathcal{J}_{n\mathrm{I}}^{B_z} &= 0.402\ \mathrm{fA/T} = \mathcal{J}_{n\mathrm{IA}}^{B_z} + \mathcal{J}_{n\mathrm{IB}}^{B_z}\\ &= (0.621 - 0.219)\ \mathrm{fA/T},\\ \mathcal{J}_{n\mathrm{II}}^{B_z} &= -19.946\ \mathrm{pA/T} = \mathcal{J}_{n\mathrm{IIA}}^{B_z} + \mathcal{J}_{n\mathrm{IIB}}^{B_z}\\ &= (-3.688 - 16.258)\ \mathrm{pA/T}.\end{aligned} \tag{43}$$

The nuclear ring-current susceptibility calculated for toluene is compared to the one obtained for toluene calculated in the limit of a very high potential barrier that prevents the torsion of the methyl with respect to the phenyl group. The susceptibility as a function of the barrier height in Fig. 7 shows that the rigid-rotor limit is reached already for rather small barriers of $V_b \approx 10$ kJ/mol. The asymptotic value of the susceptibility in the rigid-rotor limit is -18.639 pA/T. Figure 7 confirms that high torsion barriers tend to increase the absolute values of the positive paratropic contributions, i.e., they diminish the total nuclear ring-current susceptibility. Thus, (relatively) large values of the total nuclear ring-current susceptibility profit from low torsion barriers.

IV. CONCLUSION

The theory of magnetically induced nuclear ring currents in torsional molecules, with the torsion axis oriented along the magnetic field, has been developed and applied to toluene. In the derivation of the expression for the nuclear ring current, we assumed that the Born-Oppenheimer approximation (BOA) holds. The wave functions for the torsional and rotational motions were obtained by solving the Schrödinger equation with cyclic boundary conditions for the torsional or rotational nuclear motions using the BOA potential energy surface of the torsion and neglecting the other nuclear degrees of freedom. In our model, we considered bare nuclei and neglected couplings with electronic ring currents.

We found that magnetically induced nuclear ring currents consist of diatropic and paratropic components, corresponding to nuclei rotating in the classical and nonclassical directions, respectively. The assignment is analogous to the diatropic and paratropic contributions to magnetically induced electronic ring currents in molecules [6,9]. The nonclassical paratropic component depends on the torsional and rotational wave function, whereas the classical diatropic component does not. Thus, the tropicity of nuclear ring currents is easily assessed, whereas the tropicity of magnetically induced electronic ring currents can be determined from the circulation direction with respect to the magnetic-field vector by following the current density vector around the vortex [6,11,35].

The application to toluene shows that the nuclear ring currents and their diatropic and paratropic components depend almost linearly on the magnetic-field strength at least for static magnetic fields of less than 10 T that can be created in a laboratory. Higher-order terms can be neglected when comparing with an eventual experiment. Thus, magnetically induced nuclear ring currents can be understood by studying the related ring-current susceptibility that does not depend on the magnetic-field strength.

The calculated nuclear ring-current susceptibility for toluene is $\mathcal{J}_{n,\mathrm{tot}}^{B_z} = -19.946$ pA/T, consisting of 99.9% of the classical diatropic contribution. The nonclassical paratropic contribution to the ring-current susceptibility is only 0.402 fA/T. It is nonzero but negligible in comparison to the diatropic contribution. Analysis of the influence of the torsional barrier showed that the small paratropic contribution is due to the low barrier of 0.0583 kJ/mol of toluene [26]. For a high barrier greater than 10 kJ/mol, the paratropic contribution approaches 1.306 pA/T, which is obtained in the rigid-rotor limit. Another factor that affects the paratropic contribution to the nuclear ring current is the ratio between the rotating charges (Q_A and Q_B) of the fragments divided by their moments of inertia (I_A and I_B). When $Q_A/I_A = Q_B/I_B$, the paratropic contribution vanishes.

The half plane for calculating the ring-current strength can be chosen arbitrary, because the strength of the nuclear ring current passing all half planes must be the same due

to charge conservation [16]. The nuclear ring-current susceptibility of −19.946 pA/T is three orders of magnitude smaller than the electronic diatropic ring-current susceptibility of about 12 nA/T for benzene [7,36], which may be due to the ratio of 1836 between the nuclear magneton of nuclear ring currents and the Bohr magneton of electronic current densities. However, magnetically induced electronic ring-current susceptibilities are generally calculated for ring-shaped molecules whose rings are perpendicular to the direction of the external magnetic field [11]. The strength of the net electronic ring current may then be weaker than for aromatic rings, because the diatropic and paratropic contributions to the electronic ring currents may cancel as in nonaromatic molecules [36].

In the following paper [37] we investigate the electronic current density of toluene when the external magnetic field is oriented along the torsion axis as in this work. Our method to calculate magnetically induced electronic current densities is presented and the strength of the electronic current-density susceptibility is compared to nuclear ring currents.

The theoretical predictions call for experiments monitoring magnetically induced nuclear ring currents in oriented torsional molecules. The first prerequisite is to align the molecular torsion axis along the magnetic field to employ one of the experimental methods that are used for investigating magnetically induced electronic ring currents in studies of nuclear ring currents. Essentially, this means entering a white research territory.

ACKNOWLEDGMENTS

This work was supported by the National Key Research and Development Program of China (Grant No. 2017YFA0304203), Natural Science Basic Research Program of Shaanxi (Grant No. 2022JQ-062), the Program for Changjiang Scholars and Innovative Research Team (Grant No. IR_17R70), the National Natural Science Foundation of China (Grant No. 11904215), the 111 project (Grant No. D18001), the Fund for Shanxi 1331 Project, the Hundred Talent Program of Shanxi Province, the Academy of Finland through Projects No. 314821 and No. 340583, and the Swedish Cultural Foundation in Finland. M.D. thanks the Finnish Cultural Foundation for a research grant.

APPENDIX A: DERIVATION OF THE EXPRESSION FOR CALCULATING NUCLEAR RING CURRENTS

The time derivative of the nuclear probability density $\rho_n(\varphi_A, \varphi_B) = \psi^*(\varphi_A, \varphi_B)\psi(\varphi_A, \varphi_B)$ yields

$$
\begin{aligned}
i\hbar\frac{\partial\rho(\varphi_A,\varphi_B)}{\partial t} &= i\hbar\frac{\partial}{\partial t}[\psi^*(\varphi_A,\varphi_B)\psi(\varphi_A,\varphi_B)]\\
&= \psi^*(\varphi_A,\varphi_B)H\psi(\varphi_A,\varphi_B) - \psi(\varphi_A,\varphi_B)[H\psi(\varphi_A,\varphi_B)]^*\\
&= -\frac{\hbar^2}{2I_A}\frac{\partial}{\partial\varphi_A}\left(\psi^*(\varphi_A,\varphi_B)\frac{\partial}{\partial\varphi_A}\psi(\varphi_A,\varphi_B) - \psi(\varphi_A,\varphi_B)\frac{\partial}{\partial\varphi_A}\psi^*(\varphi_A,\varphi_B)\right)\\
&\quad -\frac{\hbar^2}{2I_B}\frac{\partial}{\partial\varphi_B}\left(\psi^*(\varphi_A,\varphi_B)\frac{\partial}{\partial\varphi_B}\psi(\varphi_A,\varphi_B) - \psi(\varphi_A,\varphi_B)\frac{\partial}{\partial\varphi_B}\psi^*(\varphi_A,\varphi_B)\right)\\
&\quad + ig_A\mu_N B_z\frac{\partial}{\partial\varphi_A}[\psi^*(\varphi_A,\varphi_B)\psi(\varphi_A,\varphi_B)]\\
&\quad + \mathrm{i}g_B\mu_N B_z\frac{\partial}{\partial\varphi_B}[\psi^*(\varphi_A,\varphi_B)\psi(\varphi_A,\varphi_B)],
\end{aligned}
\tag{A1}
$$

which has the form of a rotational continuity equation for molecule AB,

$$
\frac{\partial}{\partial t}\rho(\varphi_A,\varphi_B) + \frac{\partial}{\partial\varphi_A}j_A(\varphi_A,\varphi_B) + \frac{\partial}{\partial\varphi_B}j_B(\varphi_A,\varphi_B) = 0. \tag{A2}
$$

Equations (A1) and (A2) yield the expression for the magnetically induced 2D rotational probability ring-current densities of the oriented torsional molecule,

$$
\begin{aligned}
j_A(\varphi_A,\varphi_B) &= -\frac{i\hbar}{2I_A}\left[\psi^*(\varphi_A,\varphi_B)\frac{\partial}{\partial\varphi_A}\psi(\varphi_A,\varphi_B) - \psi(\varphi_A,\varphi_B)\frac{\partial}{\partial\varphi_A}\psi^*(\varphi_A,\varphi_B)\right] - \frac{g_A\mu_N B_z}{\hbar}\psi^*(\varphi_A,\varphi_B)\psi(\varphi_A,\varphi_B)\\
&\equiv j_{A\mathrm{I}}(\varphi_A,\varphi_B) + j_{A\mathrm{II}}(\varphi_A,\varphi_B),\\
j_B(\varphi_A,\varphi_B) &= -\frac{i\hbar}{2I_B}\left[\psi^*(\varphi_A,\varphi_B)\frac{\partial}{\partial\varphi_B}\psi(\varphi_A,\varphi_B) - \psi(\varphi_A,\varphi_B)\frac{\partial}{\partial\varphi_B}\psi^*(\varphi_A,\varphi_B)\right] - \frac{g_B\mu_N B_z}{\hbar}\psi^*(\varphi_A,\varphi_B)\psi(\varphi_A,\varphi_B)\\
&\equiv j_{B\mathrm{I}}(\varphi_A,\varphi_B) + j_{B\mathrm{II}}(\varphi_A,\varphi_B).
\end{aligned}
\tag{A3}
$$

Analogously, the 1D rotational continuity equation for fragment A is

$$\frac{\partial}{\partial t}\rho_{nA}(\varphi_A) + \frac{\partial}{\partial \varphi_A} j_{nA}(\varphi_A) = 0, \tag{A4}$$

with 1D nuclear density

$$\rho_{nA}(\varphi_A) = \int_0^{2\pi} \rho(\varphi_A, \varphi_B) d\varphi_B. \tag{A5}$$

Equations (A2), (A4), and (A5) yield the magnetically induced 1D rotational probability ring-current density of fragment A around the torsion axis,

$$j_{nA}(\varphi_A) = \int_0^{2\pi} j_A(\varphi_A, \varphi_B) d\varphi_B, \tag{A6}$$

and

$$j_{nB}(\varphi_B) = \int_0^{2\pi} j_B(\varphi_A, \varphi_B) d\varphi_A \tag{A7}$$

for fragment B.

The torsional and rotational ground state $\psi_{mM}(\varphi_A, \varphi_B)$ of molecule AB has quantum numbers $mM = 0$. To simplify the notation, we will omit these quantum numbers. The wave function

$$\psi(\varphi_A, \varphi_B) = \sum_{m'} c_{m'} \phi_{m'}(\varphi_A, \varphi_B) \tag{A8}$$

can be expanded in the orthogonal basis functions

$$\phi_{m'}(\varphi_A, \varphi_B) = \frac{1}{2\pi} e^{im'\varphi_A} e^{-im'\varphi_B}. \tag{A9}$$

The expression for calculations of nuclear ring currents contains the integrals

$$\begin{aligned}
&\int_0^{2\pi} \psi^*(\varphi_A, \varphi_B) \frac{\partial}{\partial \varphi_A} \psi(\varphi_A, \varphi_B) d\varphi_A \\
&= \int_0^{2\pi} \psi(\varphi_A, \varphi_B) \frac{\partial}{\partial \varphi_B} \psi^*(\varphi_A, \varphi_B) d\varphi_B \\
&= \frac{i}{(2\pi)^2} \sum_{m'n'} m' c^*_{m'} c_{n'} 2\pi \delta_{m'n'} \\
&= \frac{i}{2\pi} \sum_{m'}{}' m' |c_{m'}|^2, \\
&\int_0^{2\pi} \psi(\varphi_A, \varphi_B) \frac{\partial}{\partial \varphi_A} \psi^*(\varphi_A, \varphi_B) d\varphi_{\mathrm{A}} \\
&= \int_0^{2\pi} \psi^*(\varphi_A, \varphi_B) \frac{\partial}{\partial \varphi_B} \psi(\varphi_A, \varphi_B) d\varphi_B \\
&= -\int_0^{2\pi} \psi^*(\varphi_A, \varphi_B) \frac{\partial}{\partial \varphi_A} \psi(\varphi_A, \varphi_B) d\varphi_A \\
&= -\frac{i}{2\pi} \sum_{m'}{}' m' |c_{m'}|^2.
\end{aligned} \tag{A10}$$

Inserting Eq. (A10) into Eqs. (A3), (A6), and (A7) yields the probability ring-current densities of fragments A and B [16],

$$\begin{aligned}
J_{nA}(\varphi_A) &= j_{nA}(\varphi_A) \\
&= \frac{\hbar}{2\pi I_A} \sum_{m'}{}' m' |c_{m'}|^2 - \frac{g_A \mu_N B_z}{2\pi\hbar} \\
&= \frac{\hbar}{2\pi I_A} \sum_{m'>0}{}' m' (|c_{m'}|^2 - |c_{-m'}|^2) - \frac{g_A \mu_N B_z}{2\pi\hbar} \\
&\equiv J_{nA\mathrm{I}} + J_{nA\mathrm{II}} \equiv j_{nA\mathrm{I}} + j_{nA\mathrm{II}}, \\
J_{nB}(\varphi_B) &= j_{nB}(\varphi_B) \\
&= \frac{-\hbar}{2\pi I_B} \sum_{m'>0}{}' m' (|c_{m'}|^2 - |c_{-m'}|^2) - \frac{g_B \mu_N B_z}{2\pi\hbar} \\
&\equiv J_{nB\mathrm{I}} + J_{nB\mathrm{II}} \equiv j_{nB\mathrm{I}} + j_{nB\mathrm{II}},
\end{aligned} \tag{A11}$$

where contribution I depends on the torsional and rotational wave function and contribution II does not. Nuclear probability ring currents of electronic eigenstates are time independent. The continuity equations (A2) and (A4) imply that the angular probability ring-current density does not depend on the angle, as seen in Eq. (A11). The following relations hold for the nuclear probability current density:

$$\begin{aligned}
J_n &= J_{nA} + J_{nB} = j_{nA} + j_{nB}, \\
J_{nA} &= J_{nA\mathrm{I}} + J_{nA\mathrm{II}} = j_{nA\mathrm{I}} + j_{nA\mathrm{II}}, \\
J_{nB} &= J_{nB\mathrm{I}} + J_{nB\mathrm{II}} = j_{nB\mathrm{I}} + j_{nB\mathrm{II}}.
\end{aligned} \tag{A12}$$

The total nuclear ring currents can then be obtain by multiplying with nuclear charges

$$\begin{aligned}
\mathcal{J}_{n,\mathrm{tot}} &= \mathcal{J}_{nA} + \mathcal{J}_{nB} = Q_A J_{nA} + Q_B J_{nB} \\
&= \mathcal{J}_{n\mathrm{I}} + \mathcal{J}_{n\mathrm{II}}, \\
\mathcal{J}_{n\mathrm{I}} &= Q_A J_{nA\mathrm{I}} + Q_B J_{nB\mathrm{I}}, \\
\mathcal{J}_{n\mathrm{II}} &= Q_A J_{nA\mathrm{II}} + Q_B J_{nB\mathrm{II}}.
\end{aligned} \tag{A13}$$

The total nuclear ring current is the integrated flux through a half plane at arbitrary angle ϕ,

$$\mathcal{J}_{n,\mathrm{tot}}(\phi) = \mathcal{J}_{nA}(\varphi_A = \phi) + \mathcal{J}_{nB}(\varphi_B = \phi). \tag{A14}$$

The same holds for the expression in Eq. (A12), since the nuclear ring-current strength does not depend on the angle of the integration plane.

APPENDIX B: ELECTRONIC STRUCTURE CALCULATIONS

We have carried out density-functional theory calculations of the torsion barrier with the B3LYP functional using the def2-TZVP and def2-QZVP basis sets [27–29]. The semiempirical D3-BJ term was employed to take dispersion interactions into account [30]. The calculations were done with TURBOMOLE 7.4 [31,32], employing the m5 integration grid [33]. The convergence criteria of the structural optimization were 10^{-6} a.u. for the gradient norm and $10^{-6} E_h$ for the energy. The convergence threshold of the electron density was 10^{-7} a.u.

The minimum structure of the staggered conformer at $\varphi = 30^\circ$ was optimized by enforcing the C_s point group symme-

try, with the (y, z) plane as the reflection plane. The relative energy of the staggered toluene was set to $V(\varphi = 30^\circ) \equiv 0$. The DEFINE module of TURBOMOLE was used for rotating the methyl group in steps of 10°. The geometries of the molecular structures were subsequently optimized while keeping the dihedral angle $\angle$HCCC = H7-C7-C1-C2 frozen.

[1] T. Grohmann, D. Haase, D. Jia, J. Manz, and Y. Yang, J. Chem. Phys. **149**, 184302 (2018).

[2] See Supplemental Material at http://link.aps.org/supplemental/10.1103/PhysRevA.106.042801 for the coordinates of the molecular structures and the notation used.

[3] D. Sundholm, M. Dimitrova, and R. J. F. Berger, Chem. Commun. **57**, 12362 (2021).

[4] S. Coriani, P. Lazzeretti, M. Malagoli, and Zanasi, Theoret. Chim. Acta **89**, 181 (1994).

[5] R. Zanasi, P. Lazzeretti, M. Malagoli, and F. Piccinini, J. Chem. Phys. **102**, 7150 (1995).

[6] P. Lazzeretti, Prog. Nucl. Magn. Reson. Spectrosc. **36**, 1 (2000).

[7] J. Jusélius, D. Sundholm, and J. Gauss, J. Chem. Phys. **121**, 3952 (2004).

[8] S. Taubert, D. Sundholm, and J. Jusélius, J. Chem. Phys. **134**, 054123 (2011).

[9] D. Sundholm, H. Fliegl, and R. J. F. Berger, WIREs Comput. Mol. Sci. **6**, 639 (2016).

[10] H. Fliegl, R. Valiev, F. Pichierri, and D. Sundholm, in *Chemical Modelling*, edited by M. Springborg and J.-O. Joswig (Royal Society of Chemistry, Cambridge, 2018), Vol. 14, Chap. 1, pp. 1–42.

[11] M. Dimitrova and D. Sundholm, in *Aromaticity: Modern Computational Methods and Applications*, edited by I. Fernández López (Elsevier, Amsterdam, 2021), Chap. 5, pp. 155–194.

[12] D. Sundholm and H. Fliegl, in *Handbook of Porphyrin Science*, edited by K. M. Kadish, K. M. Smith, and R. Guilard (World Scientific, Singapore, 2022).

[13] J. Jusélius, D. Sundholm *et al.*, GIMIC, gauge-including magnetically induced currents: A stand-alone program for the calculation of magnetically induced current density, https://github.com/qmcurrents/gimic.

[14] J. R. Gascooke, E. A. Virgo, and W. D. Lawrance, J. Chem. Phys. **142**, 024315 (2015).

[15] K. Hoki, D. Kröner, and J. Manz, Chem. Phys. **267**, 59 (2001).

[16] T. Bredtmann, D. J. Diestler, S.-D. Li, J. Manz, J. F. Pérez-Torres, W.-J. Tian, Y.-B. Wu, Y. Yang, and H.-J. Zhai, Phys. Chem. Chem. Phys. **17**, 29421 (2015).

[17] T. Grohmann and J. Manz, Mol. Phys. **116**, 2538 (2018).

[18] S. Viefers, P. Koskinen, P. Singha Deo, and M. Manninen, Physica E **21**, 1 (2004).

[19] V. M. Fomin, in *Physics of Quantum Rings*, edited by V. M. Fomin (Springer, Berlin, 2014), pp. 1–24.

[20] R. R. S. Oliveira, A. A. Araújo Filho, F. C. E. Lima, R. V. Maluf, and C. A. S. Almeida, Eur. Phys. J. Plus **134**, 495 (2019).

[21] R. Debbarma, H. Potts, C. J. Stenberg, A. Tsintzis, S. Lehmann, K. Dick, M. Leijnse, and C. Thelander, Nano Lett. **22**, 334 (2022).

[22] L. D. Landau and E. M. Lifshitz, *Quantum Mechanics: Non-Relativistic Theory* (Pergamon, London, 1981).

[23] D. B. Moss, C. S. Parmenter, and G. E. Ewing, J. Chem. Phys. **86**, 51 (1987).

[24] R. A. Walker, E. C. Richard, K.-T. Lu, and J. C. Weisshaar, J. Phys. Chem. **99**, 12422 (1995).

[25] J. R. Gascooke and W. D. Lawrance, J. Chem. Phys. **138**, 134302 (2013).

[26] V. V. Ilyushin, Z. Kisiel, L. Pszczólkowski, H. Mäder, and J. T. Hougen, J. Mol. Spectrosc. **259**, 26 (2010).

[27] A. D. Becke, J. Chem. Phys. **98**, 5648 (1993).

[28] C. Lee, W. Yang, and R. G. Parr, Phys. Rev. B **37**, 785 (1988).

[29] F. Weigend and R. Ahlrichs, Phys. Chem. Chem. Phys. **7**, 3297 (2005).

[30] S. Grimme, J. Antony, S. Ehrlich, and H. Krieg, J. Chem. Phys. **132**, 154104 (2010).

[31] R. Ahlrichs, M. Bär, M. Häser, H. Horn, and C. Kölmel, Chem. Phys. Lett. **162**, 165 (1989); current version available at http://www.turbomole.com

[32] F. Furche, R. Ahlrichs, C. Hättig, W. Klopper, M. Sierka, and F. Weigend, WIREs Comput. Mol. Sci. **4**, 91 (2014).

[33] O. Treutler and R. Ahlrichs, J. Chem. Phys. **102**, 346 (1995).

[34] R. Seip, G. Schultz, I. Hargittai, and Z. G. Szabó, Z. Naturforsch. A **32**, 1178 (1977).

[35] J. A. N. F. Gomes and R. B. Mallion, Chem. Rev. **101**, 1349 (2001).

[36] H. Fliegl, D. Sundholm, S. Taubert, J. Jusélius, and W. Klopper, J. Phys. Chem. A **113**, 8668 (2009).

[37] M. Dimitrova, D. Jia, J. Manz, and D. Sundholm, following paper, Phys. Rev. A **106**, 042802 (2022).